Available on CMS information server

CMS NOTE 1998/028

The Compact Muon Solenoid Experiment

CMS Note

Mailing address: CMS CERN, CH-1211 GENEVA 23, Switzerland

20 April 1998

HF transverse segmentation and tagging jet capability

E. Doroshkevich, V. Gavrilov, S. Kuleshov

ITEP, Moscow, Russia

Abstract

So called tagging jets and pile-up were simulated for the optimisation of the HF segmentation. The energy resolution, angular resolution and efficiency of jet reconstruction are defined for different calorimeter segmentation.

1 Introduction

High energy jets ($\overline{E_{jet}} \sim 1TeV$) will be produced at the LHC in the reaction $qq \rightarrow (WW, ZZ \rightarrow H)jj$ in the pseudo rapidity range $2 \leq |\eta| \leq 5$. The very forward calorimeter HF of the CMS detector will cover rapidity range $3 \leq |\eta| \leq 5$. At hight luminosity $10^{34}\ cm^{-2}s^{-1}$ (average number of the interactions per one bunch crossing will be 25) pile-up effects will be rather large. It is important to find an optimal HF segmentation for reliable jets reconstruction and for the effective separation tagging jets from pile-up background.

2 HF response simulation and jet finding

The jets were generated by means of the PYTHIA package in the pseudo rapidity range $3 < |\eta| < 5$. The transverse energy of the jets ranges from 15 GeV to 200 GeV. The mean transverse energy is 58 GeV. Each jet was considered as a mixture of hadrons (mainly $\pi^{\pm}$) and gammas contained in a $\eta - \phi$ cone around the direction of the initial quark which given rise to this jet. Pile-up events were defined as mixture of hard minimum bias events. The number of minimum bias events per bunch crossing was generated according to Poisson distribution with the average value 25. Finally each bunch crossing produced one tagging jet and pile-up event.

There were analysed 4 types of HF segmentation in ηxϕ space: 0.1x0.1, 0.2x0.2, 0.3x0.3 and 0.4x0.4. One should note that for given types of segmentation the number of divisions of the range of ϕ was 64, 32, 20, 16 correspondingly. The response of the HF was calculated as a sum of responses of all particles produced in bunch crossing. The beam test results of quartz fiber calorimeter [1] for initial pions were used for calculation of the response to all types of hadrons. The results for initial electrons were used for simulation of the response to gammas. For each cell of calorimeter particle shower Φ was integrated according to analytical expression [1]

$$\Phi = \int_{cell} \Phi(R)dxdy \tag{1}$$

where

$$\Phi(R) = C_1 e^{a_1 R} + C_2 e^{a_2 R}.$$

The hadron response was corrected taking into account measured in [1] e/π ratio.

The transverse energy for the pile-up events $E_t^{pile-up}$ is distributed uniformly on azimuth angle ϕ. The dependences of pile-up mean transverse energy on pseudorapidity η is shown in Fig. 1. It is a consequence that the charged particle distribution is flat in pseudorapidity and particles transverse momentum is independent on η. This dependence was approximated using function

$$E_t^{pile-up}(\eta) = P_1 - P_2 * \eta. \tag{2}$$

with parameters P_1 and P_2 listed in Table.

	0.1x0.1	0.2x0.2	0.3x0.3	0.4x0.4
P_1	1.44±0.11	5.67±0.30	11.9±0.7	22.4±1.2
P_2	0.24±0.03	0.94±0.07	1.80±0.17	3.70±0.32

For each fired cell of HF the pile-up mean transverse energy has been subtracted.

The standard UA1 jet finding algorithm [2] was used for the jet reconstruction. A search is made over all cells of the calorimeter with the transverse energy above the seed threshold $E_{T,seed}$ equals 0.75 or 1.5 or 2.25 or 3.0 GeV corresponding to given segmentation. The cell with highest transverse energy becomes first jet initiator. The cells inside cone radius $r = 0.5$ are added vectorially to initiator. Therefore the direction of the jet candidate is defined. Procedure of summing cells inside cone with smaller than 0.5 radius (e.g. 0.4) repeated around determined jet candidate direction. Final jet energy and direction are defined. If transverse energy is more than 15 GeV and total energy is more than 600 GeV this candidate named jet. This procedure was repeated until all cells above $E_{T,seed}$ have been assigned to jet. For the segmentation 0.4x0.4 we also used summing of cells around initiator in 3x3 matrix.

Note that in jet finding algorithm good developed in CDF [3] and D0 [4] experiments the parameter of cone radius variates from 0.4 to 0.7.

The radial containment of jets is shown in Fig. 2. Approximately 95% of jet energy concentrated inside cone of radius 0.3. We analysed jets with $3.5 < |\eta| < 4.5$. We selected this range of η to have cone with radius 0.5 in $\eta - \phi$ space around jet direction totally covered by the cells of the HF calorimeter.

3 Jet identification and energy resolution

Fig. 3a shows plot for determined transverse jet energy E_t^{jet} versus transverse energy $E_t^{jet-gen}$ of generated jet. This distribution consists of two parts: one part where $E_t^{jet} \sim E_t^{jet-gen}$ corresponds to correctly identified jets, the second part where E_t^{jet} is small and does not depend on $E_t^{jet-gen}$ corresponds to pile-up background. To determine more precisely criteria of jet identification it was calculated distance r in $\eta - \phi$ space between jet found and jet generated. Distribution of events on r is shown in Fig. 4. Jets with $r > r_0$ correspond to pile-up. Fig. 3b shows plot E_t^{jet} versus $E_t^{jet-gen}$ for jets with $r < r_0$. This plot confirms that this area corresponds to correctly identified jets.

In [5] it was suggested to use parameter of lateral jet size LAT:

$$LAT = \frac{\sum_{r<0.5} r_i \cdot E_i}{\sum_{r<0.5} E_i}. \quad (3)$$

Plot LAT versus E_t^{jet} for $r > r_0$ (pile-up) is shown in Fig. 5a and for $r < r_0$ (tagging jets) is shown in Fig. 5b. Solid line shows the cut which provides pile-up rejection 99% and dashed line shows rejection level 99.9%. Projection along this line, i.e. distribution on

$$W = k * E_t^{jet} - LAT \quad (4)$$

provides the best separation between jets and pile-up. Distributions on W for jets ($r < r_0$) and pile-up ($r > r_0$) are shown in Fig. 6. Using these distributions on W one can calculate efficiency of jet reconstruction for various rejection factors. Arrows in Fig. 6 show bounds W_0 for pile-up rejection 99% and 99.9%.

Efficiency of the jet reconstruction is calculated as

$$efficiency = \frac{N(r < r_0, W > W_0)}{N(r < r_0)}. \quad (5)$$

The efficiency of jet reconstruction is shown in Fig. 7 for the pile-up rejection 99% and 99.9%.

Fig. 8 shows the results of simulation of jet transverse energy resolution as a function of E_t^{jet}.

Jet transverse energy resolution and jet angular resolution for different calorimeter granularityes are shown in Fig. 9.

4 Conclusion

It has been suggested method for jets reconstruction and rejection of pile-up in CMS HF calorimeter. The efficiency of jet reconstruction smoothly depends on HF calorimeter transverse segmentation. The most sensitive value with respect to segmentation is angular resolution. The segmentation up to 0.26x0.26 (in ηxϕ space) which is equivalent to 8x24 lattice could be considered for the design of HF calorimeter.

5 Acknowledgements

We would like to thank D.Green for the initialisation of this work, A.Ferrando for fruitful discussions and D.Litvinsev for his active help in simulations.

References

[1] N.Akchurin et al., CMS TN/95-144.

[2] B.Flauger, K.Meier, Snowmass, 1990, 128

[3] CDF Collaboration, F.Abe et.al., Phys.Rev.Let. **62**,613 (1989), Phys.Rev.Let. **75**,1017 (1995)

[4] D0 Collaboration, Abachi et.al., Phys.Rev.Let. **72**,2332 (1994), Phys.Rev.Let. **75**,3618 (1995), Phys.Rev.Let. **78**,3818 (1997)

[5] Yu.Gershtein, CMS TN/95-099, CMS TN/96-094

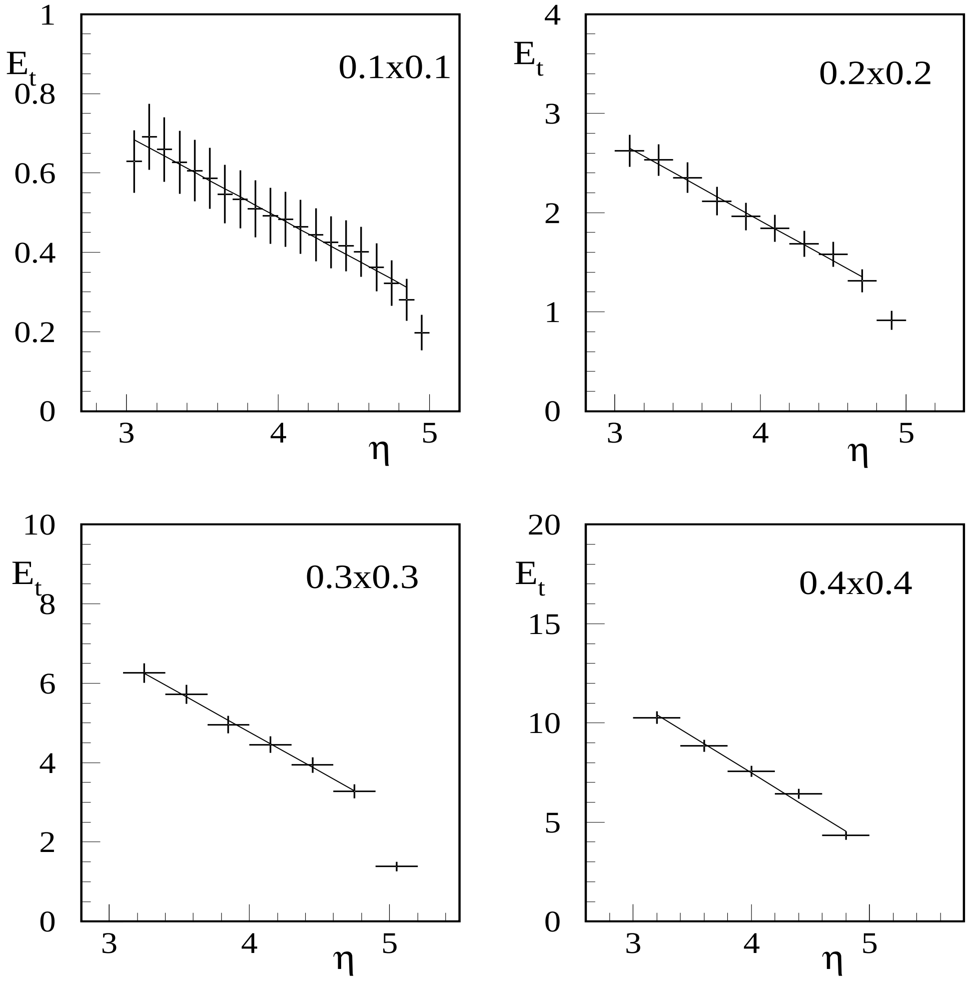

Figure 1: The dependence of pile-up on pseudorapidity

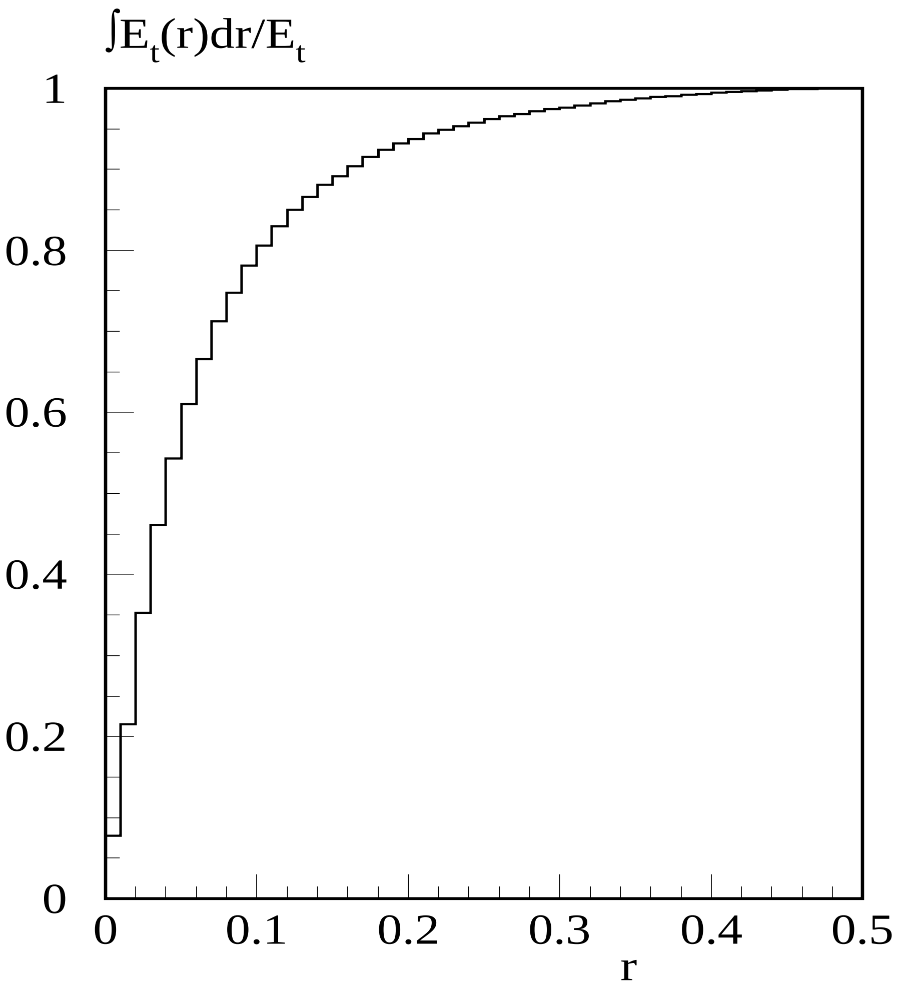

Figure 2: Jets containment

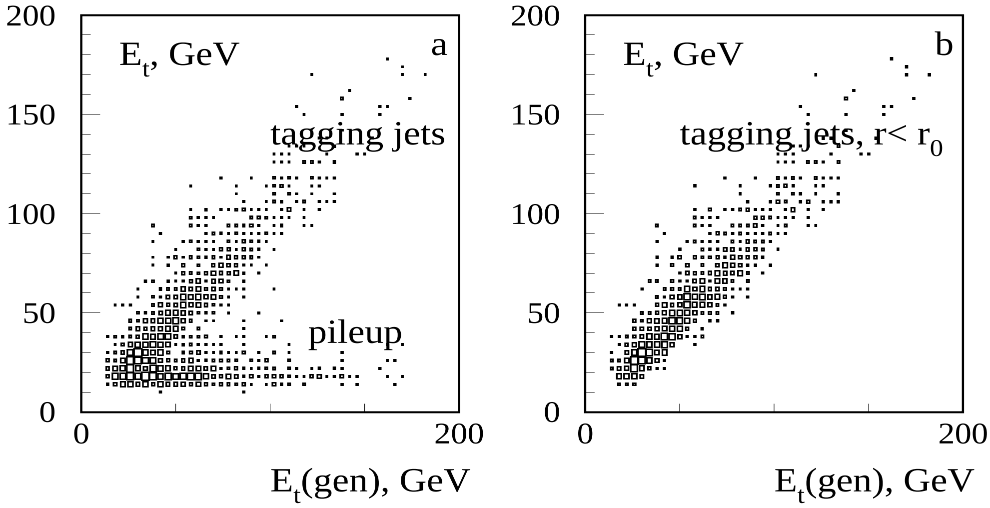

Figure 3: Jet energy vs generated jets energy

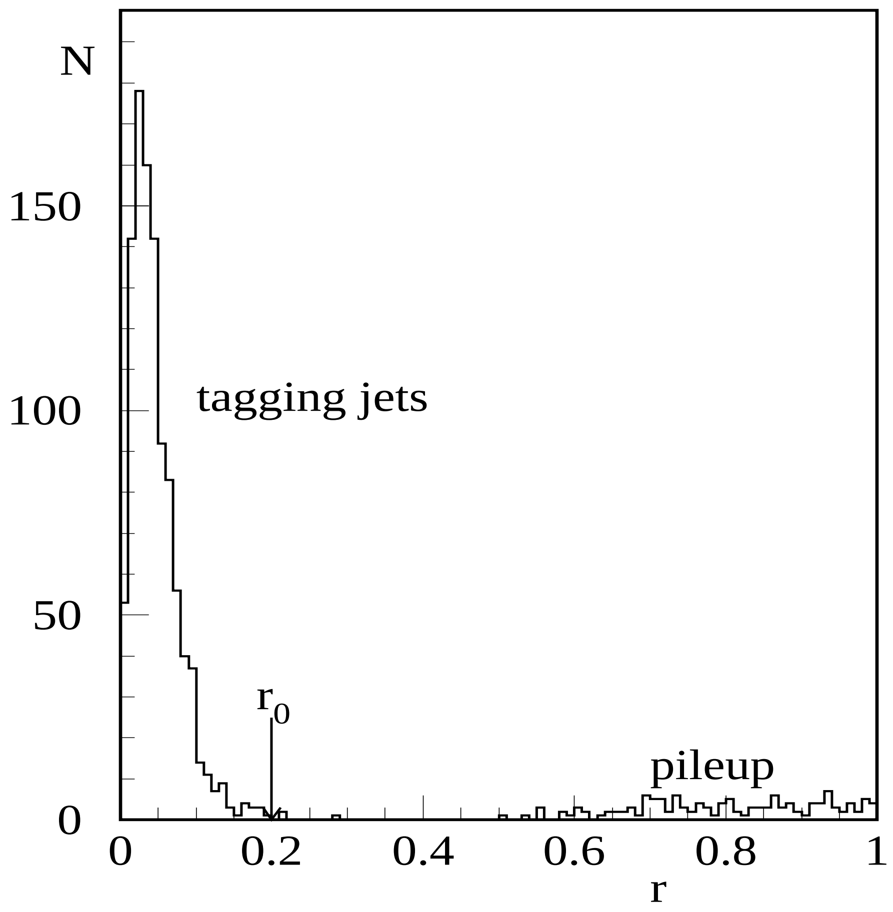

Figure 4: Distribution on r

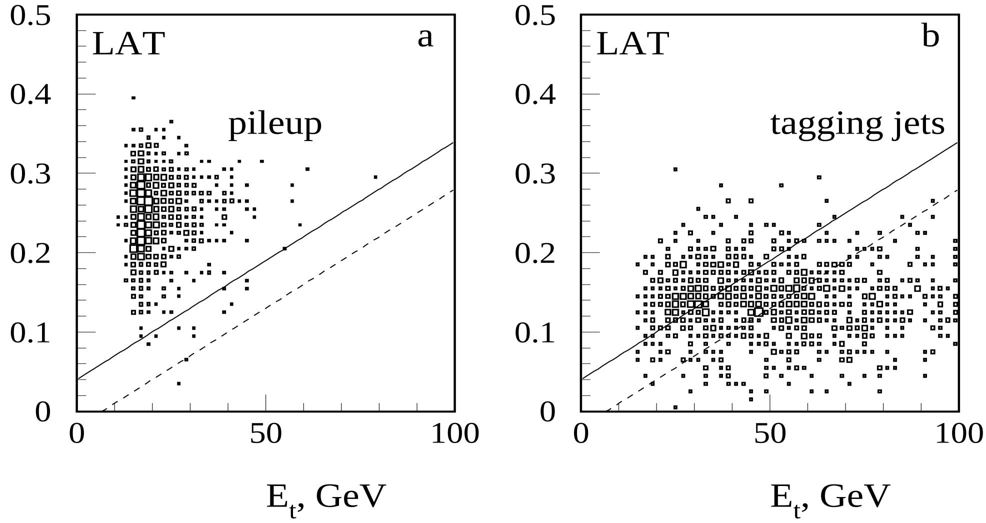

Figure 5: LAT versus E_t^{jet} for $r > r_0$ a) and for for $r < r_0$ b)

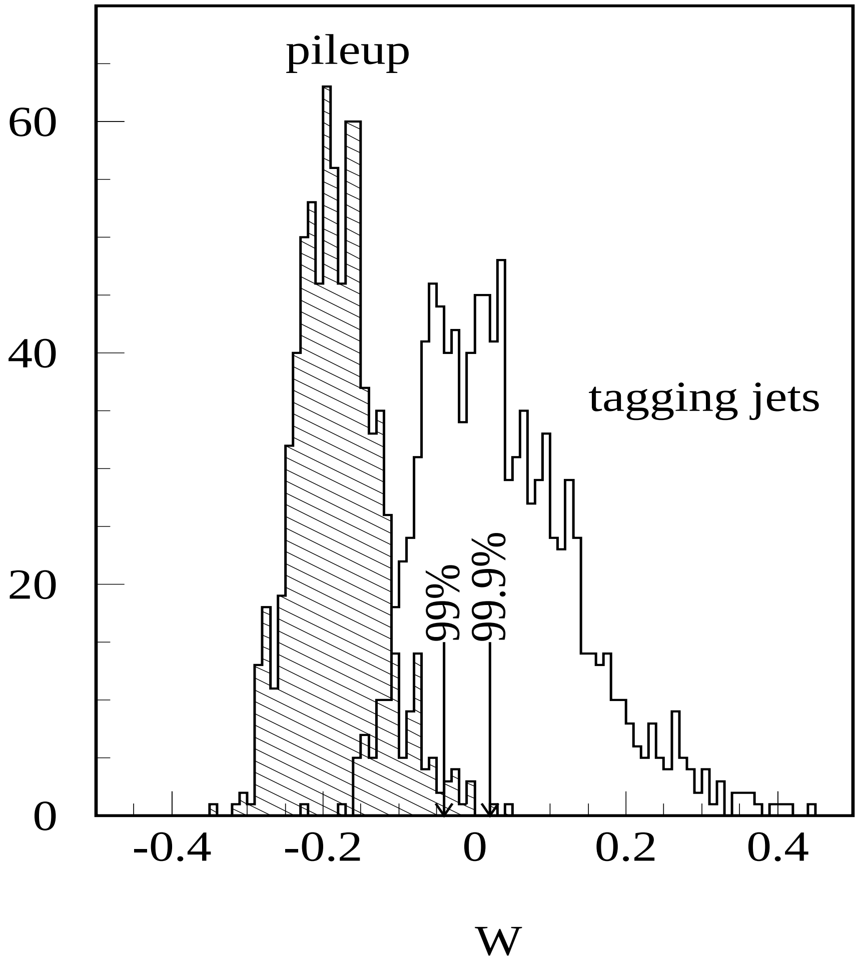

Figure 6: Distribution on W

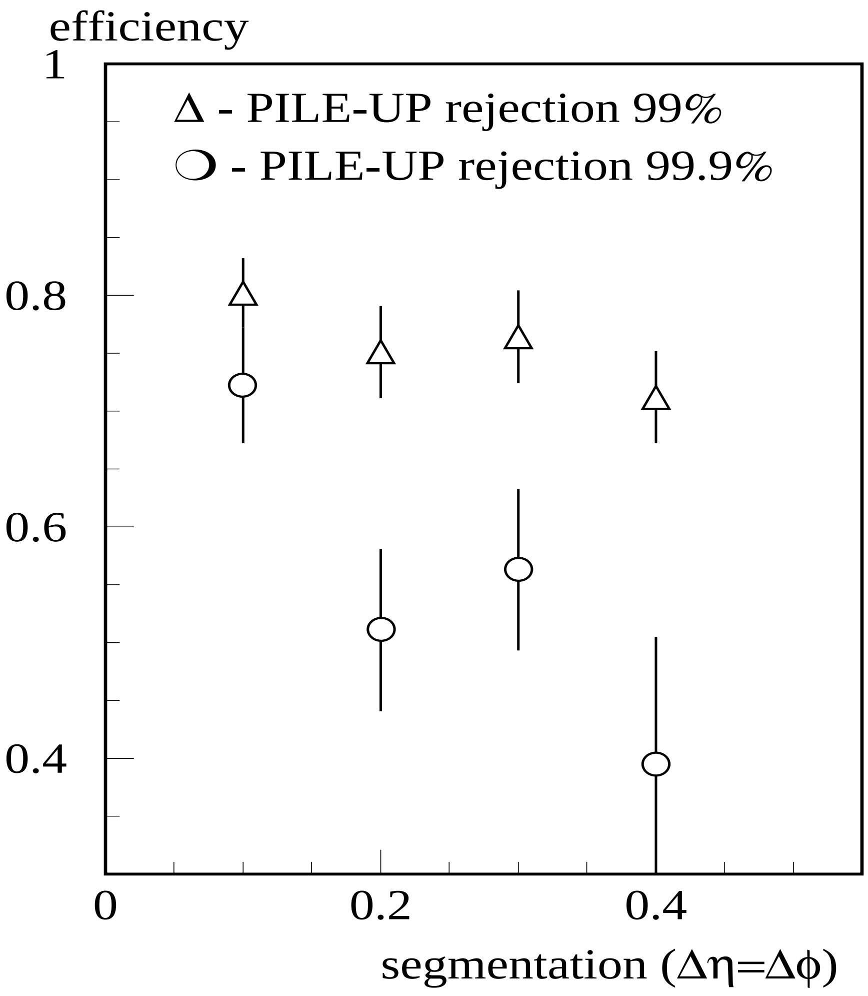

Figure 7: Efficiency of jet reconstruction

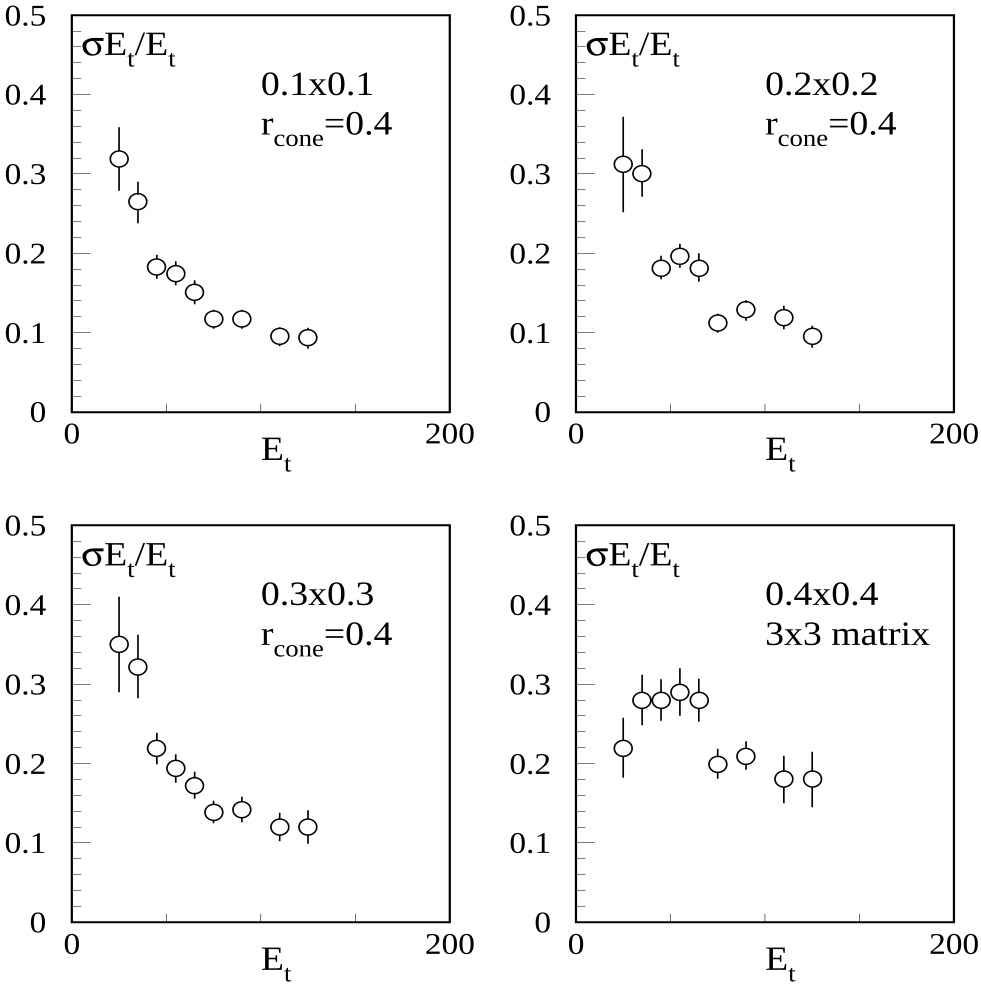

Figure 8: Jet transverse energy resolution vs E_t

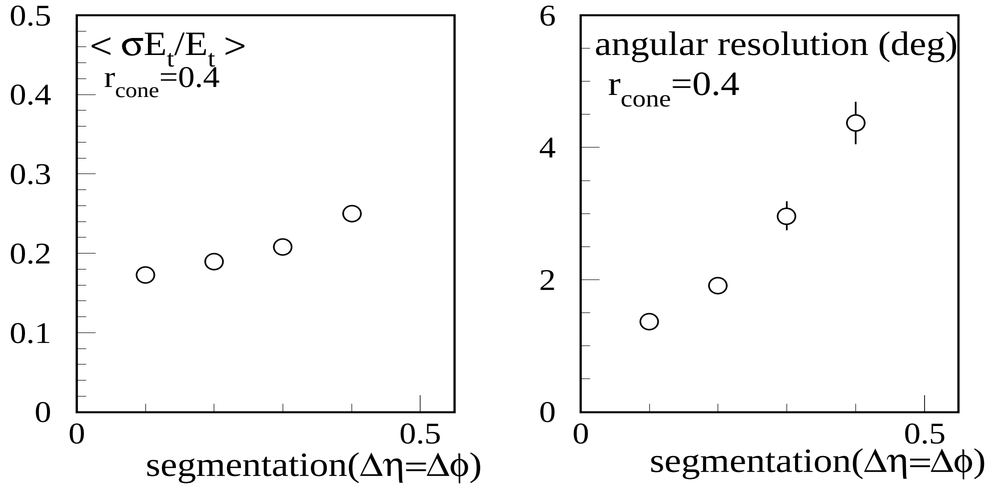

Figure 9: Energy resolution and angular resolution